Title

High-speed OTDM and WDM networks using traveling-wave electroabsorption modulators

Journal

IEEE Journal of Selected Topics in Quantum Electronics, 13(1)

ISSN

1077-260X

Authors

Chou, H F

Bowers, J E

Publication Date

2007

Peer reviewed

High-Speed OTDM and WDM Networks Using Traveling-Wave Electroabsorption Modulators

Hsu-Feng Chou, *Member, IEEE*, and John E. Bowers, *Fellow, IEEE*

(Invited Paper)

***Abstract*—We describe the design and performance of a number of elements based on traveling-wave electroabsorption modulators (TW-EAMs) in optical time-division-multiplexing (OTDM) and wavelength-division-multiplexing (WDM) networks. The incorporation of traveling-wave (TW) electrode design into electroabsorption modulators (EAMs) relieves the resistance–capacitance (*RC*) bandwidth limitation common to lumped components, enabling higher operation speed without shortening the device. As a result, high-speed operation can be combined with essential modulator characteristics such as modulation efficiency and extinction ratio. While significant modulation bandwidth has been achieved, a lesser known aspect is that the TW electrode also provides an extra dimension for improving and enabling functionalities beyond broadband modulation. This new dimension originates from the distributed effect of the TW design and its interactions with distinctive EAM properties. This paper reviews such developments in recent years with specific applications for optical signal processing in OTDM and WDM networks. The covered functionalities include various optical gating operations for OTDM, regenerative wavelength conversions for WDM, and clock recovery.**

***Index Terms*—Clock recovery, electroabsorption, optical signal processing, optical time-division multiplexing (OTDM), traveling-wave (TW), wavelength-division multiplexing (WDM).**

I. Introduction

OVER the past few decades, fiber-optic communications have made significant progress in providing higher transmission capacity with lower cost. The success of the Internet, which already changed human society globally, benefited from the developments in fiber-optics technology. Given the ~100% per year growth observed in the past few years [1], Internet traffic is expected to increase by a thousand times in the next ten years, which poses a severe challenge to the present optical network. To scale for future traffic, the optical network needs to handle higher data rates and larger capacity while offering more flexibility. The most promising solution is an optical network that utilizes optical signal processing in the *time*, *wavelength*, and *space* domains. The specific technologies involved are, respectively, optical time-division multiplexing (OTDM) [2], wavelength, division multiplexing (WDM) [3], and large-scale photonic cross connects (PXC) [4]. Even though impressive transmission speed and capacity has been demonstrated using OTDM [5] and WDM [6], many challenges remain ahead for both technologies. For OTDM, it is crucial to develop compact components and subsystems with reduced complexity for practical deployment. On the other hand, the flexibility of WDM networks would be greatly improved if efficient and compact regenerative wavelength converters are available. This paper reviews the design and application of traveling-wave electroabsorption modulators (TW-EAMs) that can provide novel solutions in response to the demands of the future optical networks.

Manuscript received August 3, 2006; revised September 21, 2006. This work was supported by the Defense Advanced Research Projects Agency (DARPA) CS-WDM program.

H.-F. Chou was with the Department of Electrical and Computer Engineering, University of California, Santa Barbara, CA 93106 USA. He is now with LuminentOIC Inc., Chatsworth, CA 91311 USA (e-mail: Hsu-Feng.Chou@ieee.org).

J. E. Bowers is with the Department of Electrical and Computer Engineering, University of California, Santa Barbara, CA 93106 USA (e-mail: bowers@ece.ucsb.edu).

Digital Object Identifier 10.1109/JSTQE.2006.887152

II. TW EAMs and Their Unique Properties

The electroabsorption modulator (EAM) is a compact, efficient, and integrable component for fiber-optic communications. It utilizes either the Franz–Keldysh effect in bulk material, or the quantum-confined Stark effect in a multiple-quantum-well (MQW) structure to change the absorption of light according to the applied electric field [7]. MQW structures are widely used for their higher modulation efficiency, but the wavelength dependence is generally higher than for bulk material. The general advantages of EAMs over other types of modulators include: 1) a small device dimension, usually on the order of a few hundred micrometers or less; 2) a lower driving voltage due to its highly efficient and nonlinear electro-optical (E-O) transfer function; and 3) the possibility of monolithic integration with other semiconductor components. EAMs with lumped electrodes have been demonstrated to exhibit a small-signal 3-dB bandwidth over 40 GHz [8].

A critical design issue of the EAM is the tradeoff between the modulation bandwidth and efficiency. The bandwidth of a lumped-electrode EAM is determined by the resistance–capacitance (*RC*) time constant. To enable high-speed broadband modulation, the active waveguide length (and width) must be short in order to keep the capacitance low. For example, in [8], a 40-Gb/s device is only 63 μm long and extra-passive optical waveguides are necessary to extend the device size for easier handling. The main concern of a short active length is the reduced modulation efficiency (expressed in dB/V), which can result in a higher driving voltage. In addition, the total extinction ratio is reduced. For broadband modulation, 10 dB of dynamic extinction ratio may be adequate, but for applications like optical gating in OTDM, very high extinction ratios are required. Another issue for a short device is the reduced optical power handling capability, which is particularly critical for radio frequency (RF) photonic links.

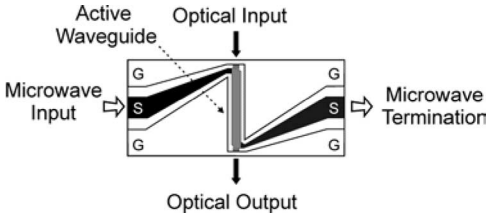

Fig. 1. Schematic diagram of a TW-EAM [13]. In our designs, the active waveguide length can vary from 100 to 600 μm and the ground–signal–ground microwave coplanar waveguide feed lines are 500 μm long.

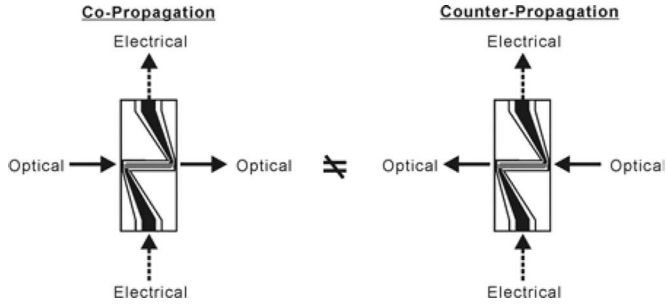

Fig. 2. One consequence of the distributed effect. The two configurations may have different optical outputs in high-frequency operation.

To overcome the tradeoff between bandwidth and device length, EAMs with traveling-wave (TW) electrodes were developed [9]–[15], where the bandwidth is not limited by lumped *RC* and the device length can be longer with a higher bandwidth. A typical implementation is illustrated schematically in Fig. 1. In the TW design, the driving signal propagates through the active waveguide, which is in fact a microwave transmission line. The junction capacitance of the EAM is no longer modeled as a lumped load but becomes distributed, particularly at high frequencies. With a longer device length, the modulation efficiency can be kept high so that only a low driving voltage is required to reach a certain dynamic extinction ratio. For example, 30-dB/V peak modulation efficiency, 1-Vpp (Volt peak-to-peak) driving voltage for error-free 10-Gb/s operation, and 14-dBm optical saturation power have been reported on a 300-μm-long InGaAsP-based TW-EAM [13]. Theoretically, the bandwidth and the useful device length of TW-EAM are only limited by the microwave loss and the velocity mismatch between the lightwave and the microwave, and both determine how long the lightwave can be effectively modulated by the microwave driving signal [16], [17]. Another limiting factor is the increase of optical scattering loss with device length, which can degrade the insertion loss of TW-EAM. Recently, an undercut-etching-active-region waveguide structure was reported to reduce both the optical and the microwave losses by reducing the scattering loss and the cladding layer resistance [18].

A critical challenge for TW-EAM is a low characteristic impedance of 25 Ω or below in the active waveguide, which causes reflections when driven by a 50-Ω source and limits the modulation bandwidth. The low impedance of the active waveguide originates from the tradeoff between the junction capacitance with several critical device parameters such as optical and microwave losses as well as the driving voltage [16]. Low impedance terminations in the range of 12 Ω to 35 Ω are required to optimize the bandwidth. For example, a bandwidth of 43 GHz was measured on a 450-μm-long device with a 13-Ω termination [14]. One way to increase the device impedance is to use a segmented transmission line design to obtain a composite impedance of 50 Ω [19]. Flat response up to 50 GHz was measured. Another practical solution is to use custom-made low impedance electronics to drive the TW-EAM. A recent development is a dual-depletion-region epilayer designed to reduce the junction capacitance, while keeping all the applied field drop across the MQW region to reduce driving voltage [20]. The reduction of junction capacitance increases the characteristic impedance and reduces the microwave loss and velocity mismatch.

Even though the TW design has been successful in extending the modulation bandwidth, its benefits in applications other than broadband modulation are not fully explored. To make the best use of TW-EAMs in building more compact and efficient subsystems, their unique properties should be explored and utilized. These unique properties include distributed effect due the TW design, generation of photocurrent, and nonlinear and engineerable E-O transfer function. The proper blending of these properties is the basis of TW-EAM-based optical signal processing.

A. Distributed Effect

The most significant implication of the TW design is that there is a *finite* length inside the TW-EAM, which generates an extra dimension for device optimization. This is particularly true when the operation frequency is raised and the microwave wavelength is comparable to the device dimension. For example, at 40 GHz, the microwave quarter wavelength is around 375 μm inside the TW-EAM reported in [13], which means that the microwave distribution may not be even across a 300-μm-long active waveguide. As a result, both the interactions in *time* and in *space* between the lightwave and the microwave should be taken into consideration. This is known as the distributed effect in TW-EAM [21].

TW operation can be observed [22] by contrasting copropagation and counterpropagation of the optical and microwave signals (Fig. 2). The copropagation configuration is preferred in terms of output power and the shortest generatable optical pulsewidth. The difference between the two configurations reduces when the operation frequency or the device length decreases. Nevertheless, even at low frequencies, a longer active waveguide with TW electrode still demonstrates the distributed effect in applications like wavelength conversion and will be discussed in Section V.

B. Photocurrent Generation

EAMs inherently generate photocurrents. The use of an EAM simultaneously as a modulator as well a photodetector has been reported in several scenarios [23]. This is a useful property through which it is possible to combine several

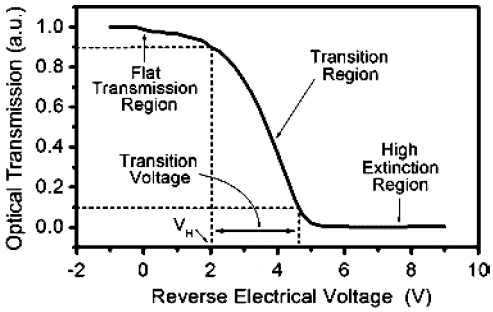

Fig. 3. E-O transfer function of an EAM.

functionalities within a single TW-EAM. Note that for applications in broadband modulation, a strong photocurrent inside the active waveguide should be avoided, since it can lead to a reduction of effective voltage supplied to the active region and degrades the large signal dynamic extinction ratio, even before the active region is saturated by a high optical injection [24].

C. Nonlinear and Engineerable E-O Transformation

The E-O transfer function of an EAM is mainly determined by the material design, and scaled by structural factors such as device length, electrode design, and waveguide geometries. Many efforts have been focused on lowering the polarization dependence by using strain-compensated MQW [10]. A typical EAM E-O transfer function is shown in Fig. 3 on a linear scale, where three transmission regions can be identified: 1) high extinction ($< 10\%$); 2) transition (10% to 90%); and 3) flat transmission ($< 90\%$). In general, the transition voltage should be small to achieve high modulation efficiency and low driving voltage. The slope of the transfer function varies point-to-point due to the nonlinear nature of electroabsorption. Nevertheless, it is possible to find certain points with minimized distortion for high dynamic range RF photonic link [25]. Normally, the voltage at which the transition begins (V_H in Fig. 3) is designed close to 0 V at the operating wavelength in order to reduce excess heating. However, if V_H can be shifted towards higher reverse voltage, more flat transmission region can be utilized without forward biasing the TW-EAM, which is very useful for signal reshaping [26].

III. Gating Operations in OTDM Networks

The most important form of optical signal processing in OTDM networks is optical gating. Specific functionalities include *optical pulse generation*, *demultiplexing*, and *add–drop multiplexing*. Numerous technologies based on fibers, semiconductor optical amplifiers (SOAs), and EAMs have been proposed and demonstrated. Brief reviews can be found in [2]. An EAM is an ideal choice for optical gating, since even a sinusoidal electrical driving signal is sufficient to generate a short gating window due to the highly nonlinear E-O transfer function of the EAM. This is a significant advantage in simplicity over all-optical gates, where an optical pulse source is required in addition to the gate itself. Other advantages include power efficiency, small size, and the ability to monolithically integrate

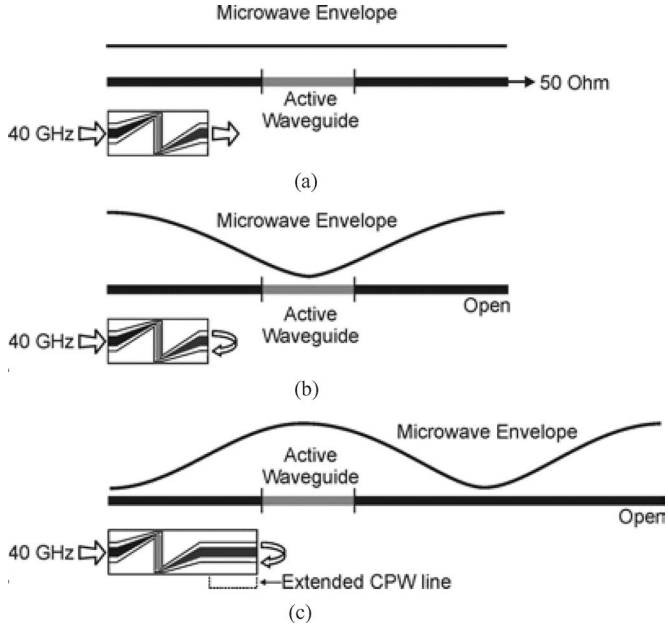

Fig. 4. Schematic of microwave envelope in (a) traveling-wave mode; (b) and (c) standing-wave enhanced mode with different termination lengths.

with lasers, amplifiers, and photodetectors. However, to operate at high OTDM bit-rates of 160 Gb/s and beyond, the requirements on gating window width and extinction ratio are stringent and the performance of electrically-driven EAM optical gates needs to be further improved.

There are four factors that determine the gating window shape of an EAM: the *modulation efficiency* and the *total extinction ratio* of the device, and the *waveform* and the *amplitude* of the driving signal. TW-EAMs can be longer than a lumped EAM and gain advantages in modulation efficiency and total extinction ratio. When a high base rate such as 40 Gb/s is adopted, the available electrical driving signal is most likely just a sinusoidal wave. Therefore, the remaining factor that can be improved is the amplitude of the driving signal.

Since there is typically an impedance mismatch between the low impedance of the TW-EAM and a 50-Ω source, the microwave amplitude in the active waveguide can be smaller than desired. One way to increase the microwave amplitude is to use two microwave amplifiers and drive the device from opposite terminals [27]. For single-frequency operation, this is equivalent to forming a standing wave along the microwave transmission line inside the TW-EAM, where the maximum swing can be doubled in the ideal case. An alternative approach is to generate the standing wave using an open termination instead of an extra amplifier, which is called the *standing-wave enhanced mode* of TW-EAM [28].

As can be understood from Fig. 4, it is crucial to adjust the spatial phase of the standing wave so that the maximum swing happens in the active waveguide. By fitting the measured results with a theoretical model, it is found that getting an even microwave distribution across the active waveguide is as important as increasing the maximum swing [28]. This indicates that at high frequencies, the distributed effect is an important issue. On

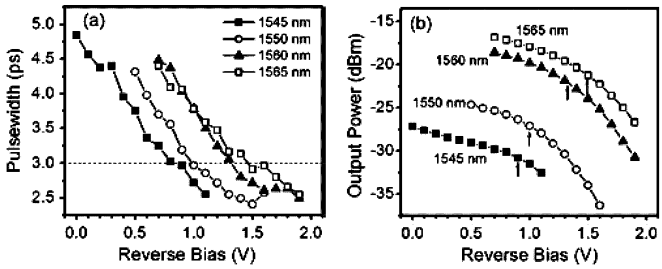

Fig. 5. 40-GHz optical pulse generation results using a standing-wave enhanced TW-EAM at 2 dBm of optical input. (a) Pulsewidth. (b) Output power. The arrows indicate the points where the pulsewidth is 3 ps.

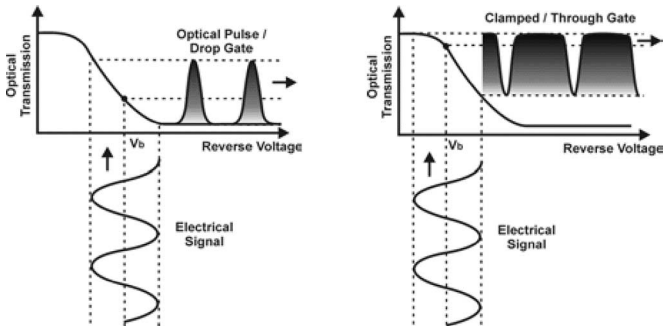

Fig. 6. Gating window shape of EAM. (a) High reverse bias for drop gate. (b) Low reverse bias for through gate. V_b: bias voltage.

the other hand, when the spatial phase of the standing wave has been properly adjusted for a specific frequency, the microwave coupling efficiency may not be optimal at the same time due to the fact that the active waveguide has a lower impedance. Techniques such as tuned stubs can be utilized to improve the microwave coupling within a narrow bandwidth [15], [29]. At lower frequencies where the impedance mismatch problem is not as severe, the standing wave enhanced mode has been shown to reduce the driving voltage by half for 80- to 10-Gb/s demultiplexing [30].

Short optical pulses can be generated when a continuous wave (CW) is being gated by the TW-EAM, a way of profiling the gating window shape. Fig. 5 shows the results of the 40-GHz optical pulse generation using a standing-wave enhanced TW-EAM (without impedance matching). Optical pulses < 2.5 ps can be generated, indicating the capability of optical demultiplexing from over 160 Gb/s down to 40 Gb/s. Even shorter pulses can be achieved, if the microwave coupling efficiency be improved further. For this particular TW-EAM, the optical insertion loss is hard-limited by 12 dB of optical coupling loss, measured using the approach reported in [31] that utilizes both transmission and photocurrent data. Waveguide structures such as spot-size converters would help to improve the fiber-to-fiber insertion loss [32]. The current 40-GHz TW-EAM pulse source can be multiplexed to 160 Gb/s using alternating-polarization multiplexing, which requires ≤ 3 ps pulses [33]. However, for single-polarization multiplexing, ≤ 2 ps pulses are needed and nonlinear pulse compressions would be required with the present performance [34].

When the repetition rate (OTDM base rate) of the optical gate is lower, the electrical driving signal itself can be pulsed, which contains higher frequency harmonics. For example, when a 20-GHz sinusoidal wave is added in phase to a 10-GHz wave, the result is a 10-GHz pulse-like signal sharper than the original 10-GHz wave. Using a 10-GHz and a 20-GHz sinusoidal wave to drive the TW-EAM from opposite electrical ports, the optical gating window can be shorter than 5.7 ps, which enabled 160- to 10-Gb/s single-stage demultiplexing with 1-dB power penalty [35]. This technique is more difficult to implement at higher base rates like 40 Gb/s, since even the first harmonic is as high as 80 GHz.

An interesting development of TW-EAM-based optical gate is the monolithic integration of a surface illuminated unitraveling-carrier photodiode (UTC-PD) and an in-plane TW-EAM [36]. The TW-EAM is directly driven by the photocurrent signal from the UTC-PD and operates like an all-optical device. Since there is no external microwave connection, the impedance of the microwave transmission lines inside the device can be matched to that of the TW-EAM in order to reduce multiple reflections. A 320- to 10-Gb/s optically-gated demultiplexing was demonstrated with 800-fs control pulses [37]. This is another example of the harmonic driving technique mentioned above, since a rich amount of harmonics is excited by the short control pulse. It is essential that the electrical bandwidth of the interconnect between the UTC-PD and the TW-EAM be sufficiently high to support many harmonics. Other optically-controlled gating operations such as retiming, sampling, and wavelength conversion have also been demonstrated with such a device [36].

OTDM add–drop multiplexing requires an additional gating window that is complementary to that of demultiplexing; instead of transmitting a certain channel, it removes one while bypassing all the others, which is termed as a "through gate." All-optical polarization rotation techniques based on fiber or SOA is an elegant way to implement both gates simultaneously [38], [39]. Electrically-driven EAMs can provide the two gates individually and was originally demonstrated with a 40-Gb/s line rate and 10-Gb/s base rate [40]. As shown in Fig. 6, the gating window shape of the EAM can switch between the two states, drop and through, simply by changing the bias point. However, there must be a wide enough flat transmission region to clamp the top of the gating window when the driving signal is a sinusoidal wave. This ensures that the through channels are reasonably equal after passing the gate. Scaling such operations to 160-Gb/s is demanding. It is easier for electrically-driven EAMs to meet these requirements with a 40-Gb/s base rate, since the duty cycle can be relaxed by four times as compared to that with a 10-Gb/s base rate. Using two optimized standing-wave enhanced TW-EAMs, a contrast ratio of 21.6 dB and a gating window of 11.7 ps was measured for the through gate, while the window width is 5.2 ps for the drop gate. Error-free operation on all channels is achieved with an average power penalty of 1 dB [41]. This is by far the only demonstration of semiconductor-based add–drop multiplexing with a 40-Gb/s base rate. It still remains a challenge to operate SOA-based approaches with a 40-Gb/s base rate due to the slow carrier

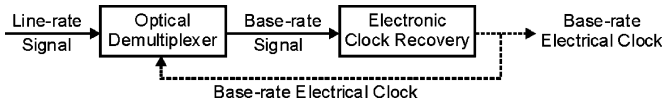

Fig. 7. Concept of scaled OTDM clock recovery.

recovery dynamics. New developments in quantum-dot SOA may provide possibilities of improved performance.

IV. Clock Recovery

In digital communication, clock recovery is essential to acquire synchronization at a network node or at the receiver end. Electronic phase-locked loop (PLL)-based clock recovery is a mature and widely used technique to recover a low-jitter clock. However, there are two major challenges: 1) in an OTDM signal, the clock tone is at the line-rate frequency, which is inherently out of the reach of electronics and 2) the lock acquisition time may not be fast enough for burst mode or packet signals, especially at 40 Gb/s and above.

Many all-optical or optoelectronic techniques have been developed in recent years to deal with these challenges. All-optical injection-locking techniques based on integrated semiconductor devices are very attractive for their small dimension and high-speed potential [42], [43]. For instance, a mode-locked laser diode can be injection-locked by an optical 160-Gb/s return-to-zero (RZ) signal and generates 160-GHz optical clock pulses [42]. This type of clock recovery is ideal for high-speed all-optical amplitude, reshaping, and retiming (3-R) regeneration at the *line rate* [44]. It is relatively difficult for these all-optical injection-locked approaches to lock at the base rate, because subharmonic tones are either not present or very low in an OTDM signal. Unfortunately, base-rate clocks are essential for demultiplexing and add–drop multiplexing. Assistive techniques can be used to improve the performance but at the expense of increased complexity [45], [46].

In terms of subharmonic clock recovery, a more commonly used approach is the combination of an optical demultiplexer and an electronic clock recovery that operates at the base rate [47], [48]. The concept of this scaled OTDM clock recovery is depicted in Fig. 7. In this approach, the optical demultiplexer brings the line-rate signal down to the base rate, at which the electronic clock recovery is able to handle. However, the demultiplexer is driven by the clock recovered by the electronic clock recovery. This extra feedback loop makes the locking acquisition process more complicated than that of the original base-rate operation. Assuming that the electronic clock recovery circuit is a standard PLL, a theoretical model can be developed to study the phase-locking dynamics [49]. The results show that: 1) there exists an optimal demultiplexing window width that optimizes the lock-in range; 2) the optimal lock-in range is inversely proportional to the number of multiplexing; and 3) with an optimal demultiplexing window width, the average lock-in time is independent of the number of multiplexing, but dependent on the ratio of frequency detuning to the lock-in range. In short, the best possible performance can be achieved when the demultiplexing window width is chosen properly. For example, if the signal pulsewidth is 50% of the line-rate bit-slot, the optimal demultiplxing window width is around 37%. To scale to a very high line rate, the stability of the base-rate oscillator is critical, since the lock-in range is considerably reduced and very little drift in frequency can be allowed. Variations of this approach using balanced detection are also reported [50]–[52].

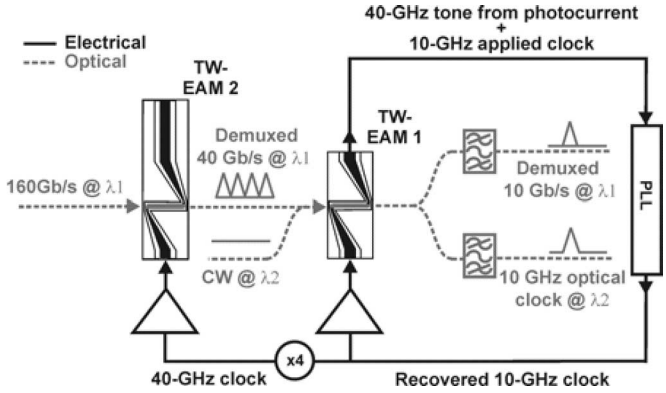

Fig. 8. Scaled simultaneous clock recovery and demultiplexing [53].

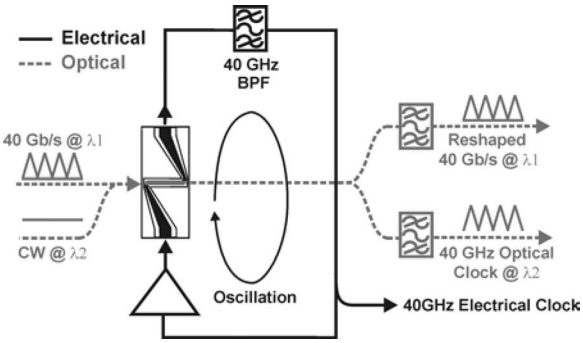

Fig. 9. TW-EAM ring oscillator clock recovery [54].

A reverse-biased EAM can be used as a photodetector to enable simultaneous functions. Fig. 8 shows an implementation of the scaled OTDM clock recovery [53] illustrated in Fig. 7. The PLL circuit takes the 40-Gb/s photocurrent signal detected by TW-EAM 1 and recovers a synchronized clock at 10 GHz, which is then multiplied to 40 GHz to drive a 160- to 40-Gb/s demultiplexer (TW-EAM 2, standing-wave enhanced). The recovered 10-GHz clock has a low jitter (224 fs) close to that of the transmitter clock (216 fs). The unique part of this setup is that the recovered 10-GHz clock can be fed back into TW-EAM 1 from another electrical port to drive it as an optical gate for 40- to 10-Gb/s demultiplexing and 10-GHz optical clock generation. The applied 10-GHz electrical clock is filtered out at the input of the PLL and does not interfere with clock recovery. As a result, three simultaneous functions, electrical and optical clock recovery, as well as demultiplexing are realized at the same time using a single TW-EAM. The power penalty for using the recovered clock is less then 0.5 dB, measured on the demultiplexed 10-Gb/s signal.

As illustrated in Fig. 9, a further evolution of TW-EAM-based clock recovery is the construction of an electrical ring oscillator using a TW-EAM as part of the ring [54], which requires

fewer components than PLL-based clock recovery. The clock synchronization is achieved by injection-locking the ring oscillator using the photocurrent signal generated by the TW-EAM. The oscillating electrical clock not only can be tapped for external use but also drives the TW-EAM into a synchronized optical gate, capable of providing synchronous modulation [55] in a very compact fashion. Furthermore, a synchronized optical clock can be obtained if a CW at another wavelength is coupled into the TW-EAM at the same time. When followed by an amplitude and reshaping (2-R) regenerative wavelength converter, this clock recovery subsystem can eliminate the need of an extra optical pulse source and additional timing adjustment between the clock and the signal for optical 3-R regeneration [56].

A theoretical model has been developed to describe this type of injection-locked clock recovery [56], [57]. It is found that the clock acquisition time depends closely on the physical length of the ring. Therefore, hybrid integration of TW-EAM, microwave amplifier, and high-Q filter is necessary for clock recovery in asynchronous 40-Gb/s packet switching [58]. A 40-GHz clock with 643 fs of jitter can be recovered within less than 3 ns, showing two-orders-of-magnitude improvement from the previous discrete version [57].

V. Wavelength Conversion and Regeneration for WDM Networks

The need for wavelength converters has grown significantly as the WDM network evolves. The trend of research in the past decade has been focused on the study of *all-optical* approaches based on nonlinearities in fibers, crystals, SOAs, and EAMs. Conversion speeds up to 640 Gb/s have been demonstrated using four-wave mixing in highly nonlinear fibers [59]. Nevertheless, while fiber-based approaches have the advantage in speed, semiconductor-based ones are very attractive for their smaller dimension and integrability. Specifically, those with monolithically integrated tunable lasers may provide the highest level of compactness [60], [61]. All-optical wavelength converters operating at 40 Gb/s are of particular interest in recent years, since field deployment of WDM networks with 40-Gb/s electrical time-division multiplexing (ETDM) technologies is becoming a reality, and conventional optical-electrical-optical (O-E-O) type of wavelength converters are not yet fully matured at such bit rate, especially in terms of cost, size, and power consumption.

Both cross-absorption modulation (XAM) and cross-phase modulation (XPM) of an EAM can be utilized to implement all-optical wavelength conversion. XPM-based approaches have been demonstrated up to 100 Gb/s but require an extra delayed-interferometer [62]. On the other hand, XAM-based approaches are simpler, but only demonstrated up to 40 Gb/s [63].

Conventionally, EAMs with lumped electrodes are used, where the mechanism behind XAM is the saturation of absorption due to a large number of carriers generated by a strong input signal, which causes field screening and band-filling effects. In such a *saturation mechanism*, a considerable amount of carriers must be generated to produce an appropriate extinction ratio. This imposes a requirement for very high input power and RZ signal format with a short pulsewidth. On the other hand, to enable high-speed operation, these carriers must be swept out of the active region to recover the absorption as fast as possible. Unfortunately, the sweep-out time increases with the number of carriers, which limits the operation speed [64]. If the active material of the EAM is designed to saturate easily so that the carriers required to reach saturation is lowered, the carrier escape time tends to be longer in such structures and the operation speed is still limited. As a result, EAM-based XAM wavelength converters using the saturation mechanism have inherent tradeoffs between speed, extinction ratio, and input power.

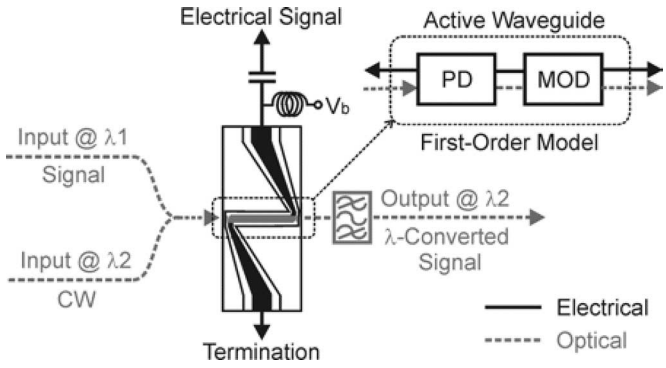

Fig. 10. Photocurrent-assisted wavelength conversion (PAW-conversion) using a TW-EAM. Insert: the first-order model; PD: photodetector; MOD: modulator.

However, when a TW-EAM is used for XAM-based wavelength conversion, there is another mechanism available in addition to absorption saturation. As shown in Fig. 10, since a TW-EAM is longer than a lumped EAM, the active waveguide can be considered as consisting of a photodetector followed by a modulator to the first order of approximation. When a strong input signal is coupled into the TW-EAM, it gets absorbed quickly by the first part of the active waveguide (the "photodetector part") and generates photocurrent signals propagating along the TW electrodes in both directions. The counterpropagating signal can be terminated or reflected, depending on the termination impedance. The copropagating signal passes through the second part of the active waveguide (the "modulator part") and changes the absorption of CW light at another wavelength. As a result, the information can be transferred from $\lambda 1$ to $\lambda 2$ without the need to saturate the TW-EAM, and consequently, free from the tradeoffs in MQW design. The photocurrent signal can subsequently be detected outside the device for signal monitoring purposes, adding an extra functionality to this approach. Since this XAM mechanism is enabled by photocurrent, this type of wavelength conversion is called *photocurrent-assisted wavelength conversion* (PAW-conversion).

The existence of the photocurrent-assisted mechanism can be verified by switching the termination of the TW-EAM between a 50-Ω oad and an open termination. It is observed that the extinction ratio of the converted optical signal is increased with an open termination. This is due to the fact that the photocurrent signal that propagates through the "modulator part" is doubled by using an open termination [65]. In an ideal case, the counterpropagating photocurrent signal should be entirely reflected and added in phase with the copropagating tributary

so that the maximal conversion efficiency can be obtained. This can be done by placing an open termination right at the optical input port.

In reality, the absorption and remodulation processes happen gradually and simultaneously along the active waveguide. A full description would require a continuously distributed model, as opposed to the first-order approximation illustrated in Fig. 10. However, if the input signal is absorbed within a short distance (typically $> 90\%$ within 100 μm), the first-order approximation is valid in general, and a numerical model that is based on it matches well with the experimental results [49]. Note that the photocurrent-assisted mechanism is another form of distributed effect that exists even at low frequencies.

It is experimentally measured in [65] that the saturation mechanism may also exist in TW-EAM, which contributes to the extinction ratio but leads to a longer carrier sweep-out time, and consequently, a reduced photodetection bandwidth. PAW-conversion was thus limited to 2.5-Gb/s nonreturn-to-zero (NRZ) operation in the original demonstration [65]. However, it is worth noting that EAM-based wavelength converters utilizing only the saturation mechanism require RZ signals with $<10\%$ duty-cycle pulses. This is due to the need of a high peak power for saturating the absorption, and also to allow time for absorption recovery between pulses. The operation speed of PAW-conversion can be further improved in two parallel ways: one deals with the fundamentals that limit the speed, while the other uses assistive means to reduce the penalty for RZ signals, which also adds extra regenerative capabilities. They are described below individually.

A. Improvements for 10-Gb/s NRZ PAW-Conversion

The most critical bottleneck of speed is the carrier escape time from the MQWs in the "photodetector part" of the active waveguide. To reduce the carrier escape time, a new generation of TW-EAM with shallower MQWs was fabricated. The material structure is compatible with the integration platform reported in [61], which means that high-level integration with a tunable laser and SOAs are technically feasible.

The 10-Gb/z NRZ eye diagrams detected by the two generations of TW-EAM are shown in Fig. 11(a) and (b), where the bias voltages are chosen to optimize the wavelength converted signal. Note that all the MQW barrier heights are reduced in the new generation and the detected eye is greatly improved compared to that of the previous generation. The E-O transfer function of the new generation shown in Fig. 11(c) also possesses two favorable properties: 1) the transition region is shifted so that the reverse bias can be set higher, which further shortens the carrier sweep-out time and 2) there is a much wider flat transmission region to reshape the converted signal through the E-O transformation, which is the same property required for generating the through gate for add–drop multiplexing [Fig. 6(b)].

The microwave terminations also need to be refined to speed up PAW-conversion. First, an open is located at the optical input end of the active waveguide so that the photocurrent travels in the copropagating direction with full strength. Secondly, a 50-Ω arallel resistor is added to the end of the active waveguide, which

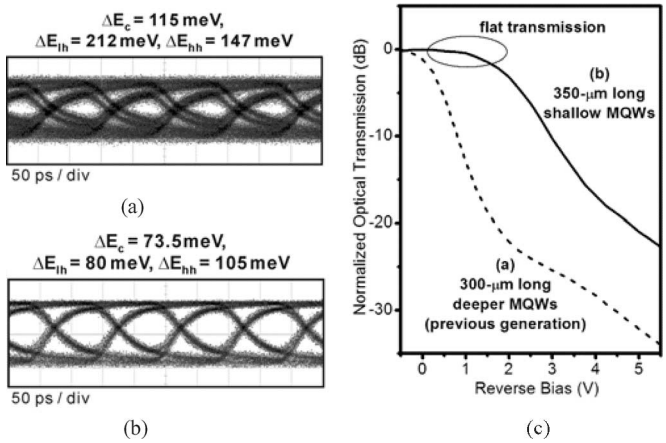

Fig. 11. 10-Gb/s NRZ eye diagram detected by TW-EAM. (a) The 300-μm-long TW-EAM with deeper MQWs at -0.7 V of bias. (b) The new generation 350-μm-long TW-EAM with shallow MQWs at -2.1 V of bias. (c) Normalized optical transfer functions.

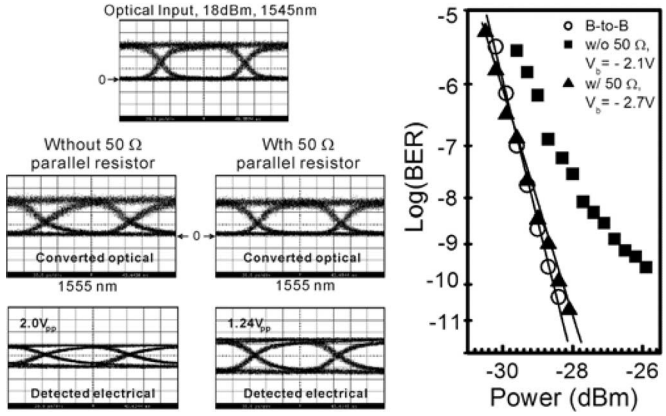

Fig. 12. Eye diagrams and bit-error-rate curves of 10-Gb/s NRZ PAW-conversion using a 350-μm-long, shallow-MQW TW-EAM, with and without a 50-Ω parallel matching resistor. The bias voltages are chosen to optimize the power penalty (20 ps/div).

helps to match the impedance of the external circuit (50 Ω) to that of the active waveguide ($< 25\ \Omega$). These arrangements are very similar to the design of a high-speed photodetector. In addition, the device length of 350 μm is optimized to balance between the E-O transfer function shape and the electrical bandwidth (limited by the multiple reflections due to residue impedance mismatch).

Fig. 12 shows the eye diagrams and the bit-error-rate (BER) curves of PAW-conversion using the 350-μm-long TW-EAM with shallow MQWs. With a 50-Ω matching resistor, the power penalty is as low as 0.1 dB for 10-Gb/s NRZ conversion. Note that the eye opening of the converted optical signal is better than that of the detected electrical signal due to the properly engineered nonlinear E-O transformation.

B. RF-driven PAW-Conversion

If an RZ signal is to be converted, the speed of PAW-conversion not only can be increased by the improvements described above, but also by an assistive technique that involves

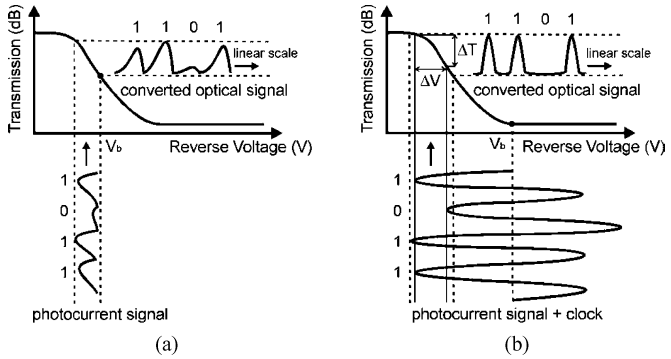

Fig. 13. E-O transformation of RZ PAW-conversion. (a) Without RF-drive. (b) With RF-drive [68].

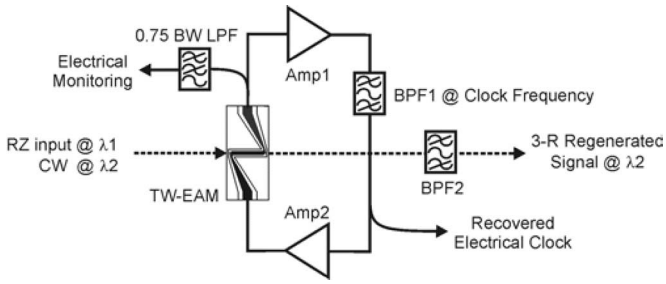

Fig. 14. Compact 3-R regenerative PAW-conversion [68].

feeding back a synchronized electrical clock. This RF-driven technique was originally proposed in [66] to reshape and retime the RZ signal that is converted using a saturation-based EAM wavelength converter. However, the regeneration performance can be even stronger when used with PAW-conversion [67].

The principle of RF-driven PAW-conversion can be explained in Fig. 13. The challenge of converting an RZ signal is that the response of the TW-EAM as a photodetector may not be fast enough to resolve the pulse shape and causes distortions such as a long falling tail in the photocurrent signal. As shown in Fig. 13(a), the converted signal carries essentially the same distortion, resulting in excess power penalty. An easy cure is to increase the reverse bias so that only the peak of the input signal is strong enough to open up the transmission. However, this would require a stronger input power and/or a shorter pulsewidth, which can be inefficient and shorten the lifetime of the device. The RF-driven approach works in a more dynamic way. As shown in Fig. 13(b), the photocurrent signal adds in phase with an applied strong sinusoidal clock signal and the long tails of the converted signal can be pulled down. The noise between bits is also suppressed. The shape and timing of the converted signal can be refined by the sinusoidal clock, while information is transferred from the input signal by the photocurrent. As a result, *retiming* and *lateral reshaping* can be obtained. In addition, the bias voltage can be increased without the need to increase the optical input power, which helps the carrier sweep-out process.

Vertical reshaping can also be realized through utilizing the nonlinear E-O transfer function of the TW-EAM. Fig. 13(b) shows that the mark level can fall in the flat transmission region of the transfer function so that noise and fluctuations in the mark can be compressed through the nonlinear E-O transformation. On the other hand, as long as the electrical eye opening ΔV is large enough so that the extinction ratio of the converted signal ΔT is better than that of the degraded input signal, noise in the space level can be reduced in the converted signal. In other words, vertical reshaping is achieved by redistributing noise through the step-like nonlinear E-O transformation.

This RF-driven approach is able to reduce the power penalty of 10-Gb/s RZ PAW-conversion from 7.5 dB down to 1 dB, even when the original deep MQW TW-EAM is used [67]. This clearly demonstrated the effectiveness of the RF-driven approach. In addition, it is demonstrated that the jitter of the converted signal can be reduced by 50% when compared to a stressed input signal, which agrees qualitatively with the numerical simulation [49].

The electrical clock required by the RF-driven PAW-conversion can be provided externally by a clock recovery unit through a properly adjusted delay. However, if the TW-EAM-based injection-locking clock recovery concept (illustrated in Fig. 9) is merged with the RF-driven PAW-conversion, a very compact 3-R regenerative wavelength converter shown in Fig. 14 can be realized [68]. Only *one* TW-EAM is necessary for simultaneous clock recovery, wavelength conversion, and regeneration. It is demonstrated that this compact setup has only 0.3 dB of power penalty for converting a clean 10-Gb/s RZ signal (using the deeper MQW TW-EAM). When injected with a degraded input signal (low extinction ratio and stressed jitter), 1 dB of negative power penalty can be obtained and the jitter is reduced after conversion. The phase between the recovered clock and the input signal is automatically aligned by the injection-locking. The jitter of the recovered clock implicitly depends on the photodetection bandwidth of the TW-EAM due to the simultaneous operation of the RF-driven PAW-conversion and the injection-locking clock recovery. A detailed analysis can be found in [49].

RF-driven PAW-conversion can be a compact regenerative wavelength converter, but there are two major challenges: 1) the regenerative strength is only moderate and has fundamental limitations on signals with more severe amplitude noise [49] and 2) a tunable optical filter is required, which is a less matured component for high-level monolithic integration. A modified O-E-O style usage of TW-EAM can overcome these issues, which will be discussed below.

The most valuable property of EAM for strong signal regeneration is its highly nonlinear and engineerable E-O transfer function, which is capable of compressing the noise and fluctuations on the mark and space levels. Fig. 15 shows a TW-EAM-based 3-R regeneration [26] setup that resembles a conventional O-E-O style of regenerator/wavelength converter. The most significant difference is that electronic signal processing circuits are not necessary since the signal is reconditioned by the transfer function of the TW-EAM, which simplifies the configuration and may reduce power consumption. Tunable optical filter is not necessary, since the input and output optical signals are isolated by electronics. This also means that the same input and output

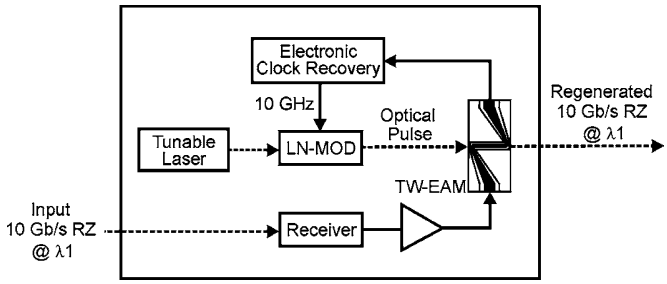

Fig. 15. Simplified O-E-O style of regenerative wavelength converter [26].

wavelength is allowed without adding another stage of wavelength converter. However, a strong driving voltage provided by electrical amplifiers is required so that the "steps" (the flat transmission and high extinction regions indicated in Fig. 3) of the E-O transfer function can be utilized for reshaping. Successful regenerations of amplified spontaneous emission (ASE) noise degraded signals have been demonstrated [26]. Numerical simulations predict that the current implementation is capable of very large number of cascades without deterministic breakdown of pulse shape [49]. Cascadability is a critical requirement in WDM networks, since a signal may need to be wavelength converted many times before reaching the final destination.

Advancements in integration technology have made it possible to integrate tunable transmitters and receivers on a single chip for wavelength conversion [61], where the EAM is directly driven by the photodetector, similar in concept to the optical gate used for OTDM gating [36]. The electrical amplifier needed for providing the voltage gain can ideally be replaced by SOAs so that hybrid integration is not required for compactness [61]. However, this would impose a higher demand on the power handling capability on the photodetector. Further reduction of transition voltage of EAM may help to relax this issue. Recent 40-Gb/s operation of integrated transmitters [69] indicates the very promising potential of these integrated O-E-O style (OEIC) wavelength converters for applications in 40-Gb/s per channel WDM networks.

VI. Conclusion

The recent developments and applications of TW-EAMs for OTDM and WDM networks are reviewed, with special focus on exploring and utilizing the device-level properties to provide novel solutions to meet system-level demands. Many of the device properties can also be found in lumped EAMs but the TW electrode design does distinguish TW-EAMs in terms of improving the gating performance and enabling novel and simultaneous functionalities. Fig. 16 summarizes most of the TW-EAM applications discussed in this paper, and the evolution and relation of technologies.

Looking forward, there are still challenges ahead for TW-EAMs and in their applications. The impedance mismatch between the active waveguide and driving electronics is the main issue that limits the bandwidth. This can be improved by new epi materials or by using lower impedance driving electronics, which may require custom design. The second issue is to

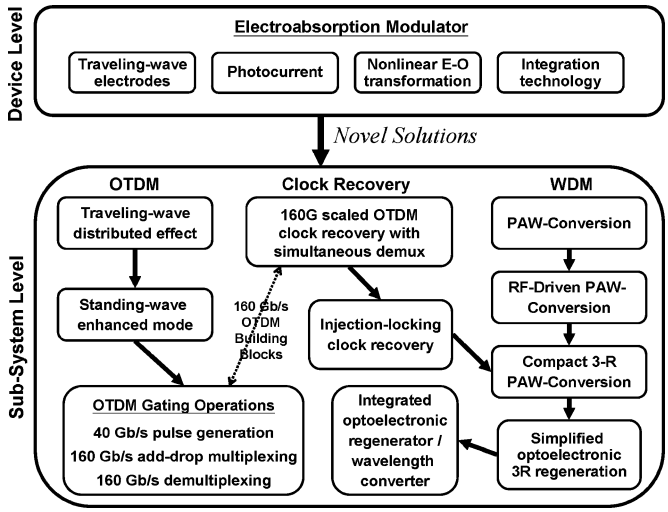

Fig. 16. Summary of TW-EAM-based applications for OTDM and WDM.

reduce the insertion loss of TW-EAMs, especially those originating from optical coupling. Waveguide spot-size converters and high-level integrations are both possible solutions.

For OTDM gating operations, the current standing-wave enhanced TW-EAMs are capable of 4:1 demultiplexing and add–drop multiplexing with a 40-Gb/s base rate, which corresponds to a line rate of 160-Gb/s. If the microwave coupling efficiency can be improved by increased characteristic impedance or impedance-matching techniques, operations at a 320-Gb/s line rate should be feasible. On the other hand, when the electrical bandwidth is sufficient, adding a harmonic at 80 GHz would help to shorten the gating widow width. One advantage of electrically-driven EAM gates is that it scales with the advancement of electronics while providing a compact configuration.

For applications in wavelength conversion in WDM networks, several variations of PAW-conversion are capable of providing compact and multifunctional solutions. With properly engineered material and microwave terminations, high-performance 10-Gb/s NRZ conversion has been achieved. Scaling the speed to 40 Gb/s has not been reported yet, but is very promising, especially with the RF-driven approach. The simultaneous operation of clock recovery and regenerative wavelength conversion using a single TW-EAM is an excellent example of reducing subsystem complexity using device-level properties. The recent advancement in photonic integration is critical to revive O-E-O style of wavelength conversion and regeneration. Up to 40-Gb/s single-chip tunable wavelength converters are very likely to mature in the coming years. However, for strong 3-R regeneration capabilities, it is not clear yet if it can be achieved without the aid of electronics (amplifiers at least).

Acknowledgment

The authors would like to thank Y.-J. Chiu, M. N. Sysak, and S. Z. Zhang for device fabrication, and Z. Hu, W. Wang, L. Rau, D. J. Blumenthal, K. Nishimura, R. Inohara, and M. Usami for helpful discussions and collaborations.

REFERENCES

[1] E. Deseveire, "Optical communications in 2025," *Eur. Conf. Opt. Commun. 2005*. Glasgow, Scotland, 2007, Plenary talk Mo2.1.3.

[2] M. Saruwatari, "All-optical signal processing for terabit/second optical transmission," *J. Sel. Topics Quantum Electron.*, vol. 6, no. 6, pp. 1363–1374, Nov./Dec. 2003.

[3] N. S. Bergano and C. R. Davidson, "Wavelength division multiplexing in long-haul transmission systems," *IEEE J. Lightw. Technol.*, vol. 14, no. 6, pp. 1299–1309, Jun. 1996.

[4] X. Zheng, V. Kaman, S. Yuan, Y. Xu, O. Jerphagnon, A. Keating, R. C. Anderson, H. N. Poulsen, B. Liu, J. R. Sechrist, C. Pusarla, R. Helkey, D. J. Blumenthal, and J. E. Bowers, "Three-dimensional MEMS photonics cross-connect switch design and performance," *J. Sel. Topics Quantum Electron.*, vol. 9, no. 2, pp. 571–578, Mar./Apr. 2003.

[5] M. Nakazawa, T. Yamamoto, and K. R. Tamura, "1.28 Tbit/s-70 km OTDM transmission using third- and fourth-order simultaneous dispersion compensation with a phase modulator," *Electron. Lett.*, vol. 36, no. 24, pp. 2027–2028, Nov. 23, 2000.

[6] K. Fukuchi, T. Kasamatsu, M. Morie, R. Ohhira, T. Ito, K. Sekiya, D. Ogasahara, and T. Ono, "10.92 Tb/s (273×40 Gb/s) triple-band/ultra-dense WDM optical-repeatered transmission experiment," presented at the *Opt. Fiber Commun. Conf.*, 2001, Paper PD24.

[7] D. A. B. Miller, D. S. Chemla, T. C. Damen, A. C. Gossard, W. Wiegmann, T. H. Wood, and C. A. Burrus, "Bandedge electroabsorption in quantum well structures: The quantum confined Stark effect," *Phys. Rev. Lett.*, vol. 53, pp. 2173–2177, 1984.

[8] T. Ido, S. Tanaka, M. Suzuki, M. Koizumi, H. Sano, and H. Inoue, "Ultra-high-speed multiple-quantum-well electro-absorption optical modulators with integrated waveguides," *J. Lightw. Technol.*, vol. 14, no. 9, pp. 2026–2034, Sep. 1996.

[9] K. Kawano, M. Kohtoku, M. Ueki, T. Ito, S. Kondoh, Y. Noguchi, and Y. Hasumi, "Polarisation-insensitive traveling-wave electrode electroabsorption (TW-EA) modulator with bandwidth over 50 GHz and driving voltage less than 2 V," *Electron. Lett.*, vol. 33, no. 18, pp. 1580–1581, Aug. 28, 1997.

[10] S. Z. Zhang, Y.-J. Chiu, P. Abraham, and J. E. Bowers, "25-GHz polarization-insensitive electroabsorption modulators with traveling-wave electrodes," *IEEE Photon. Technol. Lett.*, vol. 11, no. 2, pp. 191–193, Feb. 1999.

[11] Y. Akage, K. Kawano, S. Oku, R. Iga, H. Okamoto, Y. Miyamoto, and H. Takeuchi, "Wide bandwidth of over 50 GHz traveling-wave electrode electroabsorption modulator integrated DFB lasers," *Electron. Lett.*, vol. 37, no. 5, pp. 299–300, Mar. 1, 1997.

[12] G. L. Li, S. A. Pappert, P. Mages, C. K. Sun, W. S. C. Chang, and P. K. L. Yu, "High-saturation high-speed traveling-wave InGaAsP-InP electroabsorption modulator," *IEEE Photon. Technol. Lett.*, vol. 13, no. 10, pp. 1076–1078, Oct. 2001.

[13] Y.-J. Chiu, H.-F. Chou, V. Kaman, P. Abraham, and J. E. Bowers, "High extinction ratio and saturation power traveling-wave electroabsorption modulator," *IEEE Photon. Technol. Lett.*, vol. 14, no. 6, pp. 792–794, Jun. 2002.

[14] S. Irmscher, R. Lewen, and U. Eriksson, "InP-InGaAsP high-speed traveling-wave electroabsorption modulators with integrated termination resistors," *IEEE Photon. Technol. Lett.*, vol. 14, no. 7, pp. 923–925, Jul. 2002.

[15] J. Lim, Y.-S. Kang, K.-S. Choi, J.-H. Lee, S.-B. Kim, and J. Kim, "Analysis and characterization of traveling-wave electrode in electroabsorption modulator for radio-on-fiber application," *J. Lightw. Technol.*, vol. 21, no. 12, pp. 3004–3010, Dec. 2003.

[16] G. L. Li, C. K. Sun, S. A. Pappert, W. X. Chen, and P. K. L. Yu, "Ultrahigh-speed traveling-wave electroabsorption modulator—Design and analysis," *IEEE Trans. Microw. Theory Tech.*, vol. 47, no. 7, pp. 1177–1183, Jul. 1999.

[17] S. Nam, Y. Kim, J. Lee, M. Kim, and J. Jeong, "Performance of traveling-wave electroabsorption modulators depending on microwave properties of waveguides calculated using FDTD method," *J. Sel. Topics Quantum Electron*, vol. 9, no. 3, pp. 763–769, May/Jun. 2003.

[18] Y.-J. Chiu, T.-H. Wu, W.-C. Cheng, F. J. Lin, and J. E. Bowers, "Enhanced peformance in traveling-wave electroabsorption modulators based on undercut-etching the active-region," *IEEE Photon. Technol. Lett.*, vol. 17, no. 10, pp. 2065–2067, Oct. 2005.

[19] R. Lewen, S. Irmscher, U. Westergren, L. Thylen, and U. Eriksson, "Segmented transmission-line electroabsorption modulators," *J. Lightw. Technol.*, vol. 22, no. 1, pp. 172–179, Jan. 2004.

[20] J.-W. Shi, C.-A. Hsieh, A.-C. Shiao, Y.-S. Wu, F.-H. Huang, S.-H. Chen, Y.-T. Tsai, and J.-I. Chyi, "Demonstration of a dual-depletion-region electroabsorption modulator at 1.55-mm wavelength for high-speed and low-driving-voltage performance," *IEEE Photon. Technol. Lett.*, vol. 17, no. 10, pp. 2068–2070, Oct. 2005.

[21] Y.-J. Chiu, V. Kaman, S. Z. Zhang, and J. E. Bowers, "Distributed effects model for cascaded traveling-wave electroabsorption modulator," *IEEE Photon. Technol. Lett.*, vol. 13, no. 8, pp. 791–793, Aug. 2001.

[22] H.-F. Chou, Y.-J. Chiu, and J. E. Bowers, "40 GHz optical pulse generation using sinusoidally-driven traveling-wave electro-absorption modulator," *Electron. Lett.*, vol. 38, no. 8, pp. 379–380, Apr. 11, 2002.

[23] R. B. Welstand, S. A. Pappert, C. K. Sun, J. T. Zhu, Y. Z. Liu, and P. K. L. Yu, "Dual-function electroabsorption waveguide modulator/detector for optoelectronic transceiver applications," *IEEE Photon. Technol. Lett.*, vol. 8, no. 11, pp. 1540–1542, Nov. 1996.

[24] T. Yamanaka, H. Fukano, and T. Saitoh, "Lightwave-microwave unified analysis of electroabsorption modulators integrated with RF coplanar waveguides," *IEEE Photon. Technol. Lett.*, vol. 17, no. 12, pp. 2562–2564, Dec. 2005.

[25] B. Liu, J. Shim, Y.-J. Chiu, A. Keating, J. Piprek, and J. E. Bowers, "Analog characaterization of low-voltage MQW traveling-wave electroabsorption modulators," *J. Lightw. Technol.*, vol. 21, no. 12, pp. 3011–3019, Dec. 2003.

[26] H.-F. Chou and J. E. Bowers, "Simplified optoelectronic 3R regenerator using nonlinear electro-optical transformation in an electroabsorption modulator," *Opt. Expess*, vol. 13, no. 7, pp. 2742–2746, Apr. 2005.

[27] V. Kaman, Y.-J. Chiu, S. Z. Zhang, and J. E. Bowers, "3.7 ps pulse generation at $\geq$30 GHz by dual-drive electroabsoprtion modulator," *Electron. Lett.*, vol. 36, no. 13, pp. 1130–1132, Jun. 22, 2000.

[28] H.-F. Chou, Y.-J. Chiu, and J. E. Bowers, "Standing-wave enhanced electroabsorption modulator for 40-ghz optical pulse generation," *IEEE Photon. Technol. Lett.*, vol. 15, no. 2, pp. 215–217, Feb. 2003.

[29] T. Kuri, K. Kitayama, and Y. Takahashi, "60-GHz-band full-duplex radio-on-fiber system using two-rf-port electroabsorption transceiver," *IEEE Photon. Technol. Lett.*, vol. 12, no. 4, pp. 419–421, Apr. 2000.

[30] H.-F. Chou, Y.-J. Chiu, L. Rau, W. Wang, S. Rangarajan, J. E. Bowers, and D. J. Blumenthal, "Low power penalty 80 to 10 Gbit/s OTDM demultiplexer using standing-wave enhanced electroabsorption modulator with reduced driving voltage," *Electron. Lett.*, vol. 39, no. 1, pp. 94–95, Jan. 9, 2003.

[31] J. Shim, B. Liu, J. Piprek, and J. E. Bowers, "An improved approach of optical loss measurement using photocurrent and optical transmission in an electroabsorption modulator," *IEEE Photon. Technol. Lett.*, vol. 16, no. 6, pp. 1474–1476, Jun. 2004.

[32] Y.-S. Kang, S.-B. Kim, Y.-D. Chung, and J. Kim, "Optical coupling analysis of dual-waveguide structure for monolithic integration of photonic devices," *IEEE Photon. Technol. Lett.*, vol. 17, no. 11, pp. 2304–2306, Nov. 2005.

[33] E. Lach, M. Schmidt, K. Schuh, B. Junginger, G. Veith, and P. Nouchi, "Advanced 160 Gbit/s OTDM system based on wavelength transparent 4×40 Gbit/s ETDM transmitters and receivers," presented at the *Opt. Fiber Commun. Conf.*, 2002, Paper TuA2.

[34] B. Mikkelsen, G. Raybon, R.-J. Essiambre, A. J. Stentz, T. N. Nielsen, D. W. Peckham, L. Hsu, L. Gruner Nielsen, K. Dreyer, and J. E. Johnson, "320-Gb/s single-channel pseudolinear transmission over 200 km of nonzero-dispersion fiber," *IEEE Photon. Technol. Lett.*, vol. 12, no. 10, pp. 1400–1402, Oct. 2000.

[35] H.-F. Chou, Y.-J. Chiu, W. Wang, J. E. Bowers, and D. J. Blumenthal, "Compact 160-Gb/s demultiplexer using a single-stage electrically-gated electroabsorption modulator," *IEEE Photon. Technol. Lett.*, vol. 15, no. 10, pp. 1458–1460, Oct. 2003.

[36] S. Kodama, T. Yoshimatsu, and H. Ito, "Monolithic PD-EAM optical gate and its application to ultrafast signal processing," in *Proc. Annu. Meeting IEEE Lasers Electro-Opt. Soc.*, 2004, vol. 1, pp. 218–219, Nov. 7–11, 2004.

[37] S. Kodama, T. Yoshimatsu, and H. Ito, "320 Gbit/s error-free demultiplexing by ultrafast optical gate monolithically integrating photodiode and electroabsorption modulator," *Electron. Lett.*, vol. 39, no. 4, pp. 383–385, Feb. 20, 2003.

[38] C. Schubert, C. Schmidt, S. Ferber, R. Ludwig, and H. G. Weber, "Error-free all optical add–drop multiplexing at 160 Gbit/s," *Electron. Lett.*, vol. 39, no. 14, pp. 1074–1076, Jul. 2003.

[39] H. de Waardt, E. Tangdiongga, J. P. Turkiewicz, and G. D. Khoe, "Optical networking beyond 40 Gbit/s," presented at the *Opt. Fiber Commun. Conf.*, 2005, Paper OWK7.

[40] I. D. Phillips, A. Gloag, D. G. Moodie, N. J. Doran, I. Bennion, and A. D. Ellis, "Drop and insert multiplexing with simultaneous clock recovery using an electroabsorption modulator," *IEEE Photon. Technol. Lett.*, vol. 10, no. 2, pp. 291–293, Feb. 1998.

[41] H.-F. Chou, J. E. Bowers, and D. J. Blumenthal, "Compact 160-Gb/s add–drop multiplexer with a 40-Gb/s base rate using electroabsorption modulators," *IEEE Photon. Technol. Lett.*, vol. 16, no. 6, pp. 1564–1566, Jun. 2004.

[42] T. Ohno, K. Sato, R. Iga, Y. Kondo, T. Ito, T. Furuta, K. Yoshino, and H. Ito, "Recovery of 160 GHz optical clock from 160 Gbit/s data stream using modelocked laser diode," *Electron. Lett.*, vol. 40, no. 4, pp. 265–267, Feb. 2004.

[43] C. Bornholdt, B. Satorius, S. Schelhase, M. Mohrle, and S. Bauer, "Self-pulsating DFB laser for all-optical clock recovery at 40 Gbit/s," *Electron. Lett.*, vol. 36, no. 4, pp. 327–328, Feb. 17, 2000.

[44] S. Arahira and Y. Ogawa, "160-Gb/s OTDM signal source with 3R function utilizing ultrafast mode-locked laser diodes and modified NOLM," *IEEE Photon. Technol. Lett.*, vol. 17, no. 5, pp. 992–994, May 2005.

[45] T. Ohno, K. Sato, T. Shimizu, T. Furuta, and H. Ito, "Recovery of 40 GHz optical clock from 160 Gbit/s data using regeneratively modelocked semiconductor lasaer," *Electron. Lett.*, vol. 39, no. 5, pp. 453–455, Mar. 6, 2003.

[46] H. Yokoyama, Y. Hashimoto, H. Kurita, and I. Ogura, "Two-stage all-optical subharmonic clock recovery using modelocked semiconductor lasers," *Electron. Lett.*, vol. 36, no. 18, pp. 1577–1578, Aug. 31, 2000.

[47] D. T. K. Tong, K.-L. Deng, B. Mikkelsen, G. Raybon, K. F. Dreyer, and J. E. Johnson, "160 Gbit/s clock recovery using electroabsorption modulator-based phase-locked loop," *Electron. Lett.*, vol. 36, no. 23, pp. 1951–1952, Nov. 9, 2000.

[48] J. P. Turkiewicz, E. Tangdiongga, G. D. Khoe, and H. de Waardt, "Clock recovery and demultiplexing performance of 160-Gb/s OTDM field experiments," *IEEE Photon. Technol. Lett.*, vol. 16, no. 6, pp. 1555–1557, Jun. 2004.

[49] H.-F. Chou, "Optical signal processing using traveling-wave electroabsorption modulators" Ph.D. dissertation, Univ. California, Santa Barbara, 2005.

[50] D. T. K. Tong, B. Mikkelsen, G. Raybon, T. N. Nielsen, K. F. Dreyer, and J. E. Johnson, "Optoelectronic phase-locked loop with balanced photodetection for clock recovery in high-speed optical time-division-multiplexed systems," *IEEE Photon. Technol. Lett.*, vol. 12, no. 8, pp. 1064–1066, Aug. 2000.

[51] E. S. Awad, P. S. Cho, N. Moulton, and J. Goldhar, "Subharmonic optical clock reocvery from 160 Gb/s using time-dependent loss saturation inside a single electroabsorption modulator," *IEEE Photon. Technol. Lett.*, vol. 15, no. 12, pp. 1764–1766, Dec. 2003.

[52] C. Boerner, C. Schubert, C. Schimidt, E. Hilliger, V. Marembert, J. Berger, S. Ferber, E. Dietrich, R. Ludwig, B. Schmauss, and H. G. Weber, "160 Gbit/s clock recovery with electro-optical PLL using bidirectionally operated electroabsorption modulator as a phase comparator," *Electron. Lett.*, vol. 39, no. 14, pp. 1071–1073, Jul. 10, 2003.

[53] H.-F. Chou, Z. Hu, J. E. Bowers, D. J. Blumenthal, K. Nishimura, R. Inohara, and M. Usami, "Simultaneous 160-Gb/s demultiplexing and clock recovery by utilizing microwave harmonic frequencies in a traveling-wave electroabsorption modulator," *IEEE Photon. Technol. Lett.*, vol. 16, no. 2, pp. 608–610, Feb. 2004.

[54] Z. Hu, H.-F. Chou, J. E. Bowers, and D. J. Blumenthal, "40-Gb/s optical clock recovery using a traveling-wave electroabsorption modulator-based ring oscillator," *IEEE Photon. Technol. Lett.*, vol. 16, no. 12, pp. 2640–2642, Dec. 2004.

[55] M. Nakazawa, E. Yamada, H. Kubota, and K. Suzuki, "10 Gbit/s solution data transmission over one million kilometers," *Electron. Lett.*, vol. 27, no. 14, pp. 1270–1272, Jul. 4, 1991.

[56] Z. Hu, H.-F. Chou, K. Nishimura, M. Usami, J. E. Bowers, and D. J. Blumenthal, "Optical clock recovery circuits using traveling-wave electroabsorption modulator-based ring oscillators for 3R regeneration," *IEEE J. Sel. Topics Quantum Electron.*, vol. 11, no. 2, pp. 329–337, Mar./Apr. 2005.

[57] Z. Hu, K. Nishimura, H.-F. Chou, L. Rau, M. Usami, J. E. Bowers, and D. J. Blumenthal, "40-Gb/s optical packet clock recovery using a traveling-wave electroabsorption modulator-based ring oscillator," *IEEE Photon. Technol. Lett.*, vol. 16, no. 12, pp. 2640–2642, Dec. 2004.

[58] B. Koch, Z. Hu, J. E. Bowers, and D. J. Blumenthal, "Payload-envelope detection and label detection integrated photonic circuit for asynchronous variable-length optical packet switching with 40-Gb/s RZ payloads and 10-Gb/s NRZ labels," *J. Lightw. Technol.*, vol. 24, no. 9, pp. 3409–3417, Sep. 2006.

[59] H. Sotobayashi, W. Chujo, and T. Ozeki, "Inter-wavelegnth-band conversions and demultiplexings of 640 Gbit/s OTDM signal," presented at the *Opt. Fiber Commun. Conf.*, 2002, Paper WM2.

[60] V. Lal, M. L. Masanovic, J. A. Summers, L. A. Coldren, and D. J. Blumenthal, "Performance optimization of an In-P-based widely tunable all-optical wavelength converter operating at 40 Gb/s," *IEEE Photon. Technol. Lett.*, vol. 18, no. 4, pp. 577–579, Feb. 15, 2006.

[61] M. N. Sysak, J. W. Raring, J. S. Barton, M. Dummer, A. Tauke Pedretti, H. N. Poulsen, D. J. Blumenthal, and L. A. Coldren, "Single-chip, widely-tunable 10 Gbit/s photocurrent-driven wavelength converter incorporating a monolithically integrated laser transmitter and optical receiver," *Electron. Lett.*, vol. 42, no. 11, pp. 657–658, May 25, 2006.

[62] K. Nishimura, R. Inohara, and M. Usami, "100 Gbit/s wavelength conversion using MQW-EAM with blueshifted absorption edge," presented at the *Opt. Fiber Commun. Conf.*, 2004, Paper FD2.

[63] L. Xu, N. Chi, K. Yvind, L. J. Christiansen, L. K. Oxenløwe, J. Mørk, P. Jeppesen, and J. Hanberg, "8×40 Gb/s RZ all-optical broadcasting utilizing an electroabsorption modulator," presented at the *Opt. Fiber Commun. Conf.*, 2004, Paper MF71.

[64] S. Højfeldt, F. Romstad, and J. Mørk, "Absorption recovery in strongly saturated quantum-well electroabsorption modulators," *IEEE Photon. Technol. Lett.*, vol. 15, no. 5, pp. 676–678, May 2003.

[65] H.-F. Chou, Y.-J. Chiu, A. Keating, J. E. Bowers, and D. J. Blumenthal, "Photocurrent-assisted wavelegnth (PAW) conversion with electrical monitoring capability using a traveling-wave electroabsorption modulator," *IEEE Photon. Technol. Lett.*, vol. 16, no. 2, pp. 530–532, Feb. 2004.

[66] K. Nishimura, M. Tsurusawa, and M. Usami, "Novel all-optical 3R regeneration using cross-absorption modulation in rf-driven electroabsorption waveguide," presented at the *Eur. Conf. Opt. Commun.*, 2001, Paper We.F.2.4.

[67] H.-F. Chou, J. E. Bowers, and D. J. Blumenthal, "Novel photocurrent-assisted wavelength (PAW) converter using a traveling-wave electroabsorption modulator with signal monitoring and regeneration capabilities," presented at the *Opt. Fiber Commun. Conf.*, 2004, Paper FD4.

[68] H.-F. Chou, Z. Hu, J. E. Bowers, and D. J. Blumenthal, "Compact optical 3R regeneration using a traveling-wave electroabsorption modulator," *IEEE Photon. Technol. Lett.*, vol. 17, no. 2, pp. 486–488, Feb. 2005.

[69] J. W. Raring, L. A. Johansson, E. J. Skogen, M. N. Sysak, H. N. Poulsen, S. P. DenBaars, and L. A. Coldren, "Low drive voltage, negative chirp 40 Gb/s EA-modulator/widely-tunable laser transmitter, using quantum-well-intermixing," presented at the *Opt. Fiber Commun. Conf.*, 2006, Paper PDP26.

Hsu-Feng Chou (S'01–M'06) received the B.S. degree in physics and the M.S. degree in electro-optical engineering from the National Taiwan University (NTU), Taipei, Taiwan, R.O.C., in 1996 and 1998, respectively, and the Ph.D. degree in electrical and computer engineering from the University of California, Santa Barbara (UCSB), in 2005.

From 1998 to 2000, he was an Engineering Officer in the R.O.C. Navy. From 2005 to 2006, he was a Postdoctoral Fellow at UCSB, with research interests in coherent RF photonic link and dynamically reconfigurable optical packet switching. He is currently with LuminentOIC Inc., Chatsworth, CA, where he is working on transceiver designs. He has authored or coauthored one book chapter and over 50 papers published in various journals and conference proceedings.

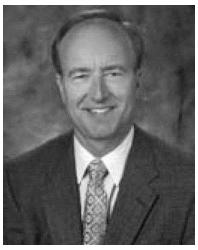

John E. Bowers (S'78–M'81–SM'85–F'93) received the M.S. and Ph.D. degrees in applied physics from Stanford University, Stanford, CA.

He is currently a Professor in the Department of Electrical Engineering, and in the Technology Management Program at the University of California, Santa Barbara. He is also the CTO and Cofounder of Calient Networks. He was with the AT&T Bell Laboratories and Honeywell before joining UCSB. His research interests include optoelectronic devices, optical switching, and transparent optical networks. He is the Cofounder of the Center for Entrepreneurship and Engineering Management, and Founder of Terabit Technology. He has authored or coauthored eight book chapters, 400 journal papers, and 600 conference papers. He holds 49 patents.

Dr. Bowers is a Fellow of the OSA and the American Physical Society. He was the recipient of the IEEE LEOS William Streifer Award and the South Coast Business and Technology Entrepreneur of the Year Award. He was an elected member of the IEEE LEOS Board of Governors, a LEOS Distinguished Lecturer, and Vice President for LEOS conferences. He is a member of the National Academy of Engineering.